Effects of system-bath entanglement on the performance of light-harvesting systems: A quantum heat engine perspective

Dazhi Xu,[1,2] Chen Wang,[2,3] Yang Zhao,[1] and Jianshu Cao[2,3,*]

[1]School of Materials Science and Engineering, Nanyang Technological University, Singapore
[2]Department of Chemistry, Massachusetts Institute of Technology, Cambridge, MA 02139 U.S.A
[3]Singapore-MIT Alliance for Research and Technology, 1 CREATE Way, Singapore 138602, Singapore

We explore energy transfer in a generic three-level system, which is coupled to three non-equilibrium baths. Built on the concept of quantum heat engine, our three-level model describes non-equilibrium quantum processes including light-harvesting energy transfer, nano-scale heat transfer, photo-induced isomerization, and photovoltaics in double quantum-dots. In the context of light-harvesting, the excitation energy is first pumped up by sunlight, then is transferred via two excited states which are coupled to a phonon bath, and finally decays to the ground state. The efficiency of this process is evaluated by steady state analysis via a polaron-transformed master equation; thus a wide range of the system-phonon coupling strength can be covered. We show that the coupling with the phonon bath not only modifies the steady state, resulting in population inversion, but also introduces a finite steady state coherence which optimizes the energy transfer flux and efficiency. In the strong coupling limit, the steady state coherence disappears and the efficiency approaches the heat engine limit given by Scovil and Schultz-Dubois in Phys. Rew. Lett. **2**, 262 (1959).

I. INTRODUCTION

With the rapid developments in measurement and manipulation of microscopic systems, quantum effects such as coherence and entanglement are often utilized to enhance the performance of microscopic devices. Even in biological systems, both experiments [1] and theoretical models [2, 3] reveal that the long-lived quantum coherence may play an important role in highly efficient energy and electron transfer processes. How biological systems, such as light-harvesting complex, preserve such long-lived coherence and how nature benefits from the coherence are two key questions that define the emerging field of quantum biology.

Taking a three-level system as a generic theoretical model, many interesting mechanisms can be well demonstrated and understood. Recently, the sunlight-induced exciton coherence is studied in a V-configuration three-level model [4, 5]. An interesting idea is to consider the energy transfer process from the perspective of heat engine [6]. For example, the coherence introduced by an auxiliary energy level can enhance the heat engine power [7, 8]. The early work considering a three-level maser model as a Carnot engine was carried out by Scovil and Schulz-DuBois [9, 10], yielding the heat engine efficiency η_0 and its relation with the Carnot efficiency. Later papers elaborately reexamined the dynamics of this model by the Lindblad master equation and showed that the thermodynamic efficiency η_0 is achieved when the output light-field is strongly coupled with the three-level system [11–13]. The quantum heat engine provides us a heuristic perspective to better understand the basic physical processes in energy transfer and presents useful insight to enhance the efficiency and output power in small systems [14–17].

In this paper, we study the polaron effects of a phonon bath on the energy transfer flux and efficiency in a generic three-level model. The canonical distribution of a thermal equilibrium system requires a negligible coupling between the system and its environment. As the coupling strength grows, the steady state of the system will no longer be canonical [18–22]. This non-canonical state actually introduces the steady state coherence into the system without refereeing to specific forms of light-matter interaction or designing exotic system configurations. The bath-induced coherent effect is investigated by the polaron-transformed Redfield equation (PTRE) [23, 24], which bridges both the weak and strong system-bath coupling regions. The difference between the steady state efficiency and strong coupling limit η_0 depends strongly on the phonon-induced coherence. Taking into account of the behaviour of both the flux and efficiency, we are able to optimize coupling and temperature in designing optimal artificial energy transfer systems.

In this paper, we first introduce the three-level model and its non-equilibrium environment in section II, and then formulate the PTRE in section III. In section IV, the polaron effects of phonon-bath on the energy transfer flux and efficiency are studied in detail. We summarize our results in the last section.

II. THREE-LEVEL SYSTEM MODEL

A. Model system

We consider the energy transfer process in the three-level system illustrated in Fig.1. The site energy of the ground state $|0\rangle$ is set to zero. The two excited energy levels $|1\rangle$ and $|2\rangle$ form a two-level system (TLS, in the

*Electronic address: jianshu@mit.edu

following the TLS is referred to the two excited states), with the corresponding site energy ϵ_1 and ϵ_2. The transition due to the dipole-dipole interaction is characterized by J. Then the three-level system is modeled by the Hamiltonian H_0 as:

$$H_0 = \sum_{i=1,2} \epsilon_i |i\rangle\langle i| + \frac{J}{2}(|1\rangle\langle 2| + |2\rangle\langle 1|). \quad (1)$$

We are interested in the transfer process in the single excitation subspace: The three-level system is firstly excited to state $|1\rangle$ by a photon field, then the excitation is transferred to state $|2\rangle$ through J (mediated by phonon modes), and finally the excitation decays to the ground state $|0\rangle$ via spontaneous radiation. The pumping and trapping processes are modeled by the interaction with the two independent photon baths, which are coupled separately with two transitions $|0\rangle \leftrightarrow |1\rangle$ and $|0\rangle \leftrightarrow |2\rangle$. The Hamiltonian of the photon baths and their interactions with the three-level system are given by

$$H_{i=\mathrm{p,t}} = \sum_k \omega_{ik} a_{ik}^\dagger a_{ik} + \left(g_{ik} a_{ik}^\dagger |0\rangle\langle i| + \mathrm{H.c.}\right), \quad (2)$$

where ω_{ik} is the eigen frequency of the bath mode described by the creation (annihilation) operator $a_{ik}^\dagger$ (a_{ik}), and its coupling strength to the excited state is g_{ik}. We note that the rotating wave approximation is applied in the system-bath interaction term. A phonon bath with creation and annihilation operators $b_k^\dagger$ and b_k of the bath mode $\omega_{\mathrm{v}k}$ is coupled to the TLS via diagonal interaction with the coupling strength of f_k. Thus, the phonon part is described by

$$H_{\mathrm{v}} = \sum_k \omega_{\mathrm{v}k} b_k^\dagger b_k + (|1\rangle\langle 1| - |2\rangle\langle 2|) \sum_k \left(f_k b_k^\dagger + \mathrm{H.c.}\right). \quad (3)$$

This microscopic three-level system immersed in the non-equilibrium environment was studied as a quantum heat pump phenomenologically without considering the details of the system-bath coupling [10]. In the case that the phonon bath is replaced by a single driving mode strongly coupled to the system, the dynamic steady states have been solved and the efficiency is given by $\eta_0 = \epsilon_2/\epsilon_1$ [12, 13]. In reality, the three-level model can be realized in both nature and laboratory. Taking the energy transfer process in photosynthetic pigment for example [Fig.2(a)], different baths could arise from different sources: the pumping light field (such as the sun-light photons) is considered as a high temperature boson bath; the trapping bath is formed by the surrounding electromagnetic environment which models the energy transfer to the reaction center; and the phonon bath with inverse temperature β_{v} describes the phonon modes coupled with the excited states. In addition, such a three-level (or more intermediate energy levels) system can be used to describe photoisomerization [Fig.2(b)], nanoscale heat transfer [25] [Fig.2(c)] or photovoltaic current in double quantum dots [26] [Fig.2(d)].

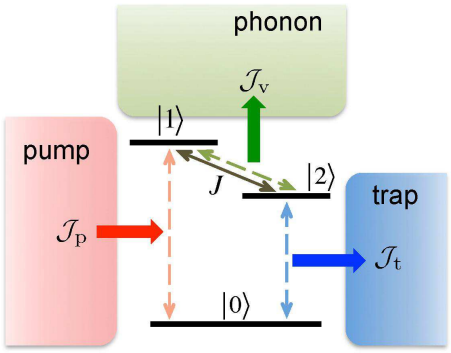

Figure 1: (color online) The system is modeled by a three-level system: its ground state $|0\rangle$ and the excited state $|1\rangle$ ($|2\rangle$) is coupled with the pumping (trapping) bath; the excited states $|1\rangle$ and $|2\rangle$ are diagonal-coupled with the phonon bath; the internal transition strength between $|1\rangle$ and $|2\rangle$ is characterized by J. The energy fluxes $\mathcal{J}_{\mathrm{p}}$, $\mathcal{J}_{\mathrm{v}}$ and $\mathcal{J}_{\mathrm{t}}$ describe the energy exchange rate of the system with the pumping, the phonon and the trapping baths, respectively. The flux into the system is defined as the positive direction.

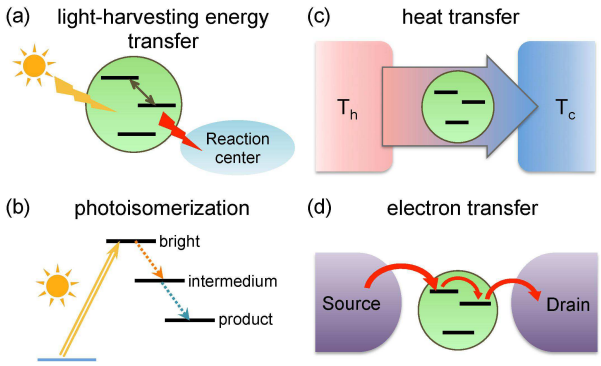

Figure 2: Realistic examples which can be studied by the three-level model with different heat baths. (a) In the photosynthesis process, the three-level system works as an antenna that captures the energy from sunlight and then transfers to the reaction center. (b) Three eigenstates manifolds in photoisomerization. The bright states are pumped by the light field, then the populations relax to the intermedium and product states in the phonon environment. (c) The heat transfer in nanoscale can also use the three-level system as a bridge connecting the high temperature and low temperature heat baths. (d) In the electron transport problem, electrons tunnel through double quantum dots which can be described by a three-level system. The quantum dot connects with a source and a drain.

In this paper, we focus on the effects of the phonon modes on energy flux and efficiency. Usually when the system-phonon bath coupling strength is not weak, the Bloch-Redfield equation approach cannot be applied. Therefore, we will introduce the polaron-transformed Redfield equation (PTRE) [23, 24], which gives reliable results from the weak to strong coupling region, to study the bath-induced coherent effects of this quantum sys-

tem.

B. Definitions of energy flux and transfer efficiency

We are interested in the energy transfer flux and efficiency of the three-level system at its non-equilibrium steady state. The steady state solution can be obtained by the master equation formally written as

$$\frac{d\rho_s(t)}{dt} = (\mathcal{L}_0 + \mathcal{L}_{\rm p} + \mathcal{L}_{\rm v} + \mathcal{L}_{\rm t})\,\rho_s(t), \tag{4}$$

which describes the dynamics of the reduced density matrix (RDM) ρ_s of the three-level system. The Liouville operator $\mathcal{L}_0$ denotes the non-dissipative term, $\mathcal{L}_{\rm p}$, $\mathcal{L}_{\rm v}$ and $\mathcal{L}_{\rm t}$ denote the dissipation effects associated with the pumping, phonon coupling, and trapping, respectively.

To quantitatively investigate the energy transfer process, we define the steady state energy fluxes by calculating the energy change of the three-level system:

$$\begin{aligned}\dot{E}(\infty) &= {\rm Tr}_s[\frac{d\rho_s}{dt}H_s]|_{t=\infty} = \sum_{i={\rm p,v,t}} {\rm Tr}_s\left[\mathcal{L}_i\left[\rho_s(\infty)\right]H_s\right] \\ &\equiv \mathcal{J}_{\rm p} + \mathcal{J}_{\rm v} + \mathcal{J}_{\rm t}. \end{aligned}\tag{5}$$

It can be shown that ${\rm Tr}_s\left[\mathcal{L}_0 H_s\right] = 0$. The three energy fluxes $\mathcal{J}_i$, $i = {\rm p, v, t}$ are defined with respect to their corresponding dissipation operator $\mathcal{L}_i$. These energy fluxes have clear physical meanings of the energy exchange rate with the pumping field, phonon environment, and trapping field, respectively. In this work, we are interested in the steady state, in Eq.(5) the fluxes are calculated with $\rho_s(\infty)$, which is obtained by solving $\dot{\rho}_s(t) = 0$. Straightforwardly, we define the energy transfer efficiency by

$$\eta = \left|\frac{\mathcal{J}_{\rm t}(\infty)}{\mathcal{J}_{\rm p}(\infty)}\right|, \tag{6}$$

which is the ratio between the output and the input energy fluxes.

Without losing generality, we assume the pumping (trapping) bath is weakly coupled with the system and can be described phenomenologically by the local Liouville operator of the Lindblad form:

$$\begin{aligned}\mathcal{L}_i[\rho_s] &= \frac{\gamma_i}{2}[(n_i+1)\left(2O_i^-\rho_s O_i^+ - \left\{O_i^+O_i^-,\rho_s\right\}\right) \\ &\quad + n_i\left(2O_i^+\rho_s O_i^- - \left\{O_i^-O_i^+,\rho_s\right\}\right)], \end{aligned}\tag{7}$$

where $i = {\rm p, t}$ refers to the two photon baths, γ_i and n_i are the corresponding decay rate and average photon number, and the system operators are defined as $O_{\rm p}^+ = |1\rangle\langle 0|$, $O_{\rm t}^+ = |2\rangle\langle 0|$. The system-phonon bath coupling will be treated more rigorously as we are interested in how this coupling affects the energy transfer over a broad range. To achieve this goal, we apply the PTRE equation, which will be introduced in the following section.

III. POLARON-TRANSFORMED REDFIELD EQUATION (PTRE)

A. Secular-Markovian Redfield equation in the polaron frame

The Redfield master equation is valid up to the second order perturbation of the system-bath interaction. In order to go beyond this weak coupling limit, polaron transformation is introduced to incorporate the high-order system-bath interaction into the dynamics of the system. Here we focus on the coupling strength between the system and phonon bath, and the polaron transformation is only related to the two excited states. Therefore, it is convenient to consider the dissipative dynamics of the TLS first, then the resulting Liouville operator describing the TLS dissipative process can be incorporated into the three-level system dynamics. We employ the Pauli matrix $\sigma_x = |1\rangle\langle 2| + |2\rangle\langle 1|$ and $\sigma_z = |1\rangle\langle 1| - |2\rangle\langle 2|$, and define the polaron transformation

$$\tilde{H}_e = e^{-i\sigma_z B/2} H_e e^{i\sigma_z B^\dagger/2} = \tilde{H}_0 + \tilde{H}_B + \tilde{V}, \tag{8}$$

where $H_e = H_0 + H_{\rm v}$ is the Hamiltonian of the TLS with the phonon bath, the collective bath operator is $B = 2i\sum_k \left(f_k b_k^\dagger - f_k^* b_k\right)/\omega_{{\rm v}k}$, and

$$\tilde{H}_0 = \frac{\epsilon}{2}\sigma_z + \frac{J}{2}\kappa\sigma_x, \tag{9}$$

$$\tilde{H}_B = \sum_k \omega_{{\rm v}k} b_k^\dagger b_k - \sum_k \frac{|f_k|^2}{\omega_{{\rm v}k}}, \tag{10}$$

$$\tilde{V} = \frac{J}{2}\left[\sigma_x\left(\cos B - \kappa\right) + \sigma_y \sin B\right]. \tag{11}$$

The transformed system-bath interaction is $\tilde{V}$, where $\epsilon = \epsilon_1 - \epsilon_2$, the expectation value of the bath operator $\kappa = {\rm Tr}_b\left[\rho_b \cos B\right]$ is subtracted as a renormalization factor, and ρ_b is the thermal state of phonon bath. The spectrum function is chosen to be super-Ohmic as $J(\omega) = 4\pi\sum_k |f_k|^2 \delta(\omega - \omega_k) = \alpha\pi\omega^3\omega_c^{-2}e^{-\omega/\omega_c}$, where ω_c is the cut-off frequency and α is a dimensionless parameter characterizing the system-bath coupling which is proportional to λ/ω_c (λ is the reorganization energy). Therefore we can obtain

$$\begin{aligned}\kappa &= \exp\left[-\int_0^\infty d\omega \frac{J(\omega)}{\pi\omega^2}\left(n_{\rm v}(\omega) + \frac{1}{2}\right)\right] \\ &= \exp\left\{\frac{\alpha}{2}\left[1 - \frac{2}{\left(\beta_{\rm v}\omega_c\right)^2}\psi_1\left(\frac{1}{\beta_{\rm v}\omega_c}\right)\right]\right\}, \end{aligned}\tag{12}$$

where $n_{\rm v}(\omega) = [\exp(\beta_{\rm v}\omega) - 1]^{-1}$ and $\psi_1(x) = \sum_{n=0}^\infty (n+x)^{-2}$ is the trigamma function.

Since the thermal average of $\tilde{V}$ is zero, then $\tilde{V}$ is of the order of bath fluctuations and is a reliable perturbation parameter. Based on this consideration, the Born-Markov approximation is applied to derive the PTRE for

TLS in the Schrodinger picture as:

$$\frac{d\tilde{\rho}_e}{dt} = -i\left[\tilde{H}_0,\tilde{\rho}_e\right] - \sum_{\alpha,\beta=z,\pm}[\Gamma^{+}_{\alpha\beta}\tau_\alpha\tau_\beta\tilde{\rho}_e + \Gamma^{-}_{\beta\alpha}\tilde{\rho}_e\tau_\beta\tau_\alpha - \Gamma^{-}_{\beta\alpha}\tau_\alpha\tilde{\rho}_e\tau_\beta - \Gamma^{+}_{\alpha\beta}\tau_\beta\tilde{\rho}_e\tau_\alpha]. \quad (13)$$

Here, $\tilde{\rho}_e$ is the RDM of the TLS in the polaron frame, and we use a new set of Pauli matrix τ_α with respect to the eigenstates of the Hamiltonian $\tilde{H}_0 = \epsilon_+ |+\rangle\langle+| + \epsilon_- |-\rangle\langle-|$:

$$\tau_z = |+\rangle\langle+| - |-\rangle\langle-|, \quad (14)$$
$$\tau_+ = |+\rangle\langle-|, \ \tau_- = |-\rangle\langle+|. \quad (15)$$

The corresponding eigenvalues and eigenstates are defined by

$$\epsilon_\pm = \pm\frac{1}{2}\sqrt{\epsilon^2 + (\kappa J)^2}, \quad (16)$$
$$|+\rangle = \cos\frac{\theta}{2}|1\rangle + \sin\frac{\theta}{2}|2\rangle, \quad (17)$$
$$|-\rangle = \sin\frac{\theta}{2}|1\rangle - \cos\frac{\theta}{2}|2\rangle, \quad (18)$$

with $\tan\theta = \kappa J/\epsilon$. The transition rates $\Gamma^{\pm}_{\alpha\beta}$ are related to the half-side Fourier transformation of the bath correlation functions

$$\Gamma^{\pm}_{\alpha\beta} = \frac{J^2}{4}\int_0^\infty dt\,\langle\xi_\alpha(\pm t)\,\xi_\beta(0)\rangle, \quad (19)$$

with

$$\xi_z(t) = \sin\theta(\cos B(t) - \kappa), \quad (20)$$
$$\xi_\pm(t) = -e^{\pm i\Delta t}[\cos\theta(\cos B(t) - \kappa) \mp i\sin B(t)] \quad (21)$$

The PTRE was firstly introduced by Silbey and coworkers [23, 24], and has been widely used in solving the strong system-bath coupling problems. Moreover, it will be shown in Sec. IV that the results given by PTRE are consistent with those given by the Redfield equation in the weak coupling limit and the Fermi's golden rule (or Förster theory) in the strong coupling limit [21, 25, 26]. Therefore, the PTRE smoothly connects the two limits, and provides a useful tool to study the intermediate coupling region where there are usually no reliable approximation methods.

B. Steady state of PTRE

For convenience, we rewrite Eq.(13) in the form of the Bloch equation

$$\frac{d}{dt}\langle\vec{\tau}(t)\rangle_e = -M\langle\vec{\tau}(t)\rangle_e + \vec{C}. \quad (22)$$

Here $\langle\vec{\tau}(t)\rangle_e^T = [\langle\tau_z(t)\rangle_e, \langle\tau_x(t)\rangle_e, \langle\tau_y(t)\rangle_e]$ with $\langle\cdot\rangle_e = \mathrm{Tr}_s[\tilde{\rho}_e(t)\cdot]$ are the elements of the density matrix $\tilde{\rho}_e(t)$,

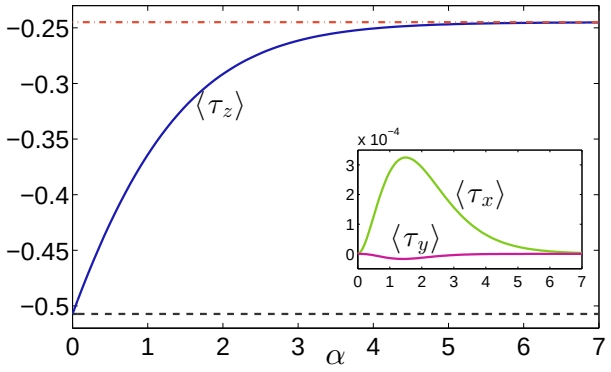

Figure 3: (color online) The steady state of TLS as a function of the system-bath coupling strength α. The steady states of the PTRE follow the canonical distribution in the polaron transformed basis, which rotates with the coupling strength α. In the weak coupling limit, the system steady state is the canonical distribution in the eigen basis (black dash line); while in the strong coupling limit, the steady state is the canonical distribution in the localized basis (red dot-dash line). The inset shows the coherent term of the steady state, which is small in the polaron transformed basis. We choose the parameters in units of J: $\epsilon_1/J = 5$, $\epsilon_2/J = 4.5$, $\omega_c/J = 5$ and $\beta_v J = 1$.

which are written in the form of the average values of the Pauli operators. The transition matrix M and the constant term $\vec{C}^T = (C_z, C_x, C_y)$ are

$$M = \begin{pmatrix} \gamma_z & \gamma_{zx} & 0 \\ \gamma_{xz} & \gamma_x & \Delta+\gamma_{xy} \\ \gamma_{yz} & -\Delta+\gamma_{yx} & \gamma_y \end{pmatrix}, \quad (23)$$
$$\vec{C}^T = (C_z, C_x, C_y), \quad (24)$$

where the eigenenergy level spacing is $\Delta = \epsilon_+ - \epsilon_-$ and the expressions of the matrix elements are given in Appendix A.

The time evolution of $\langle\vec{\tau}(t)\rangle_e$ is straightforwardly given by

$$\langle\vec{\tau}(t)\rangle_e = e^{-Mt}\left[\langle\vec{\tau}(0)\rangle_e - M^{-1}\vec{C}\right] + M^{-1}\vec{C}, \quad (25)$$

with the steady state $\langle\vec{\tau}(\infty)\rangle_e = M^{-1}\vec{C}$, and in the following we will neglect time argument ∞ when referring to the steady state for convenience. The population difference $\langle\tau_z\rangle_e$ varies with the coupling strength as shown in Fig.3. In the weak coupling limit, the TLS steady state distribution is canonical with respect to its eigen basis, i.e.,

$$\lim_{\alpha\to0}\langle\tau_z\rangle_e = \frac{1-\exp(\beta_v\sqrt{\epsilon^2+J^2})}{1+\exp(\beta_v\sqrt{\epsilon^2+J^2})}, \quad (26)$$

which is also the result $\rho_e^{\mathrm{can}} \sim \exp(-\beta_v H_0)$ given by equilibrium thermodynamics. When the system-bath coupling gradually increases, the system distribution devi-

ates from $\rho_e^{\rm can}$ and follows the Boltzmann distribution

$$\langle\tau_z\rangle_e = \frac{1-\exp(\beta_{\rm v}\sqrt{\epsilon^2+\kappa^2J^2})}{1+\exp(\beta_{\rm v}\sqrt{\epsilon^2+\kappa^2J^2})}, \quad (27)$$

with respect to the eigenenergy in the polaron transformed basis $|+\rangle$ and $|-\rangle$. In the strong coupling limit, we have

$$\lim_{\alpha\to\infty}\langle\tau_z\rangle_e = \frac{1-\exp(\beta_{\rm v}\epsilon)}{1+\exp(\beta_{\rm v}\epsilon)}, \quad (28)$$

which is the Boltzmann distribution with respect to the site energies ϵ_1 and ϵ_2 of the localized basis $|1\rangle$ and $|2\rangle$. The deviation from the canonical state $\rho_e^{\rm can}$ due to the strong system-bath coupling has been studied via the cumulant expansion method in polaron transformed thermodynamic distribution [20, 21] and from the view point of energy shell deformation [18, 19, 22].

C. Dissipative dynamics of the three-level system in the local basis

Via the PTRE we can obtain a rather accurate description of the TLS over a wide range of system-bath coupling strength. For further discussion on the property of the entire three-level system with the other two weakly coupled photon baths, all the observable quantities should be manipulated in the same frame of reference. To achieve this goal, we transform back into the frame of reference in the local basis. The diagonal terms of the system RDM are easy to deal with, as σ_z commutes with the polaron-transformation,

$$\begin{aligned}\langle\sigma_z(t)\rangle &= {\rm Tr}_{s+b}\left[\rho_{tot}(t)\,\sigma_z\right] = {\rm Tr}_s\left[\rho_e(t)\,\sigma_z\right]\\ &= {\rm Tr}_{s+b}\left[\tilde\rho_{tot}(t)\,\sigma_z\right] = {\rm Tr}_s\left[\tilde\rho_e(t)\,\sigma_z\right], \quad (29)\end{aligned}$$

where $\rho_{tot}(t)$ is the total density matrix for both the TLS and its bath, $\rho_e(t) = {\rm Tr}_b[\rho_{tot}(t)]$, and $\tilde\rho_{tot}(t) = e^{-i\sigma_z B/2}\rho_{tot}(t)\,e^{i\sigma_z B^\dagger/2}$ is the polaron-transformed total density matrix. However, the polaron transformation operator and $\sigma_x(\sigma_y)$ do not commute with each other, thus the off-diagonal terms cannot be obtained exactly. We can use the approximation $\tilde\rho_{tot}(t)\approx\tilde\rho_e(t)\otimes\tilde\rho_b$ to obtain meaningful expressions for $\langle\sigma_x(t)\rangle$ and $\langle\sigma_y(t)\rangle$. This approximation is essentially the Born approximation, which has already been used in deriving the PTRE. Based on these arguments, we have

$$\begin{aligned}\langle\sigma_x(t)\rangle &= \kappa{\rm Tr}_s\left[\tilde\rho_e(t)\,\sigma_x\right],\\ \langle\sigma_y(t)\rangle &= \kappa{\rm Tr}_s\left[\tilde\rho_e(t)\,\sigma_y\right]. \quad (30)\end{aligned}$$

According to Eqs.(17)(18), the Bloch vector $\langle\vec\sigma(t)\rangle = [\langle\sigma_x(t)\rangle, \langle\sigma_y(t)\rangle, \langle\sigma_z(t)\rangle]$ defined in the local basis of the TLS can be expressed with the quantities calculated in the polaron frame as

$$\begin{aligned}\langle\sigma_z(t)\rangle &= \cos\theta\,\langle\tau_z(t)\rangle_e + \sin\theta\,\langle\tau_x(t)\rangle_e, \quad (31)\\ \langle\sigma_x(t)\rangle &= \kappa\sin\theta\,\langle\tau_z(t)\rangle_e - \kappa\cos\theta\,\langle\tau_x(t)\rangle_e, \quad (32)\\ \langle\sigma_y(t)\rangle &= -\kappa\,\langle\tau_y(t)\rangle_e. \quad (33)\end{aligned}$$

Following from Eqs.(22)(31)(32)(33), the equations of motion for the TLS can be written in the form of $[\dot\rho_e(t)]_{ij} = \sum_{mn}[\mathcal{L}_{\rm v}]_{(ij,mn)}[\rho_e(t)]_{mn}$, then the expressions for the Liouville operator $\mathcal{L}_{\rm v}$ are straightforwardly obtained.

The equations of motion of the three-level system are derived based on Eq.(4). The Liouville operator $\mathcal{L}_{\rm v}$ with polaron effects has been obtained from the PTRE of the TLS. One thing should be noted is that in the TLS, the conservation of population gives $[\rho_e(t)]_{11}+[\rho_e(t)]_{22}=1$, while in the three-level system the conservation relation becomes $\rho_{00}(t)+\rho_{11}(t)+\rho_{22}(t)=1$, where $\rho_{ij}(t) = \langle i|\,\rho_s(t)\,|j\rangle$. The effects of the pumping and trapping baths are described by the Lindblad operator $\mathcal{L}_{\rm p}$ and $\mathcal{L}_{\rm t}$ defined in Eq.(7). Therefore, the PTRE for the three-level system is given as

$$\begin{aligned}\frac{d}{dt}\begin{pmatrix}\rho_{11}(t)-\rho_{22}(t)\\ \rho_{11}(t)+\rho_{22}(t)\\ \Re[\rho_{12}(t)]\\ \Im[\rho_{12}(t)]\end{pmatrix} &= -\bar M\begin{pmatrix}\rho_{11}(t)-\rho_{22}(t)\\ \rho_{11}(t)+\rho_{22}(t)\\ \Re[\rho_{12}(t)]\\ \Im[\rho_{12}(t)]\end{pmatrix}\\ &+ \frac{J^2}{4}\begin{pmatrix}\gamma_{\rm p}n_{\rm p}-\gamma_{\rm t}n_{\rm t}\\ \gamma_{\rm p}n_{\rm p}+\gamma_{\rm t}n_{\rm t}\\ 0\\ 0\end{pmatrix}. \quad (34)\end{aligned}$$

The matrix $\bar M$ is shown in Appendix B. The equations for the off-diagonal terms $\rho_{01}(t)$ and $\rho_{02}(t)$ are decoupled from Eq.(34) and not related with the energy flux and transfer efficiency; thus $\rho_{01}(t)$ and $\rho_{02}(t)$ will not be involved in the following discussion.

IV. ENERGY TRANSFER FLUX AND EFFICIENCY

A. Steady state flux

The steady state of the three-level system can be easily obtained from Eq.(34), which incorporates the polaron effects of the phonon bath. Then the steady state energy fluxes defined in Eq.(5) are straightforwardly given as

$$\mathcal{J}_{\rm p} = \epsilon_1\gamma_{\rm p}[n_{\rm p}\rho_{00}-(n_{\rm p}+1)\rho_{11}] - \frac{J\gamma_{\rm p}}{2}(n_{\rm p}+1)\Re[\rho_{12}] \quad (35)$$

$$\mathcal{J}_{\rm t} = \epsilon_2\gamma_{\rm t}[n_{\rm t}\rho_{00}-(n_{\rm t}+1)\rho_{22}] - \frac{J\gamma_{\rm t}}{2}(n_{\rm t}+1)\Re[\rho_{12}] \quad (36)$$

where we denote the steady state elements of RDM by $\rho_{ij} = \langle i|\rho_s(\infty)|j\rangle$ for brevity. Fig.4 presents energy fluxes with respect to α. In the extreme case that the system bath coupling is switched off ($\alpha=0$), there is no loss of excitation energy, which results in $\mathcal{J}_{\rm p} = -\mathcal{J}_{\rm t}$, suggesting the input energy flux from the pump completely flows into the trap through the three-level system (note that we chose the positive direction as that the flux flows into the system). When the coupling turns on, a portion of energy flux leaks into the phonon bath thus $\mathcal{J}_{\rm p} > -\mathcal{J}_{\rm t}$. Both the pumping and trapping energy fluxes reach their

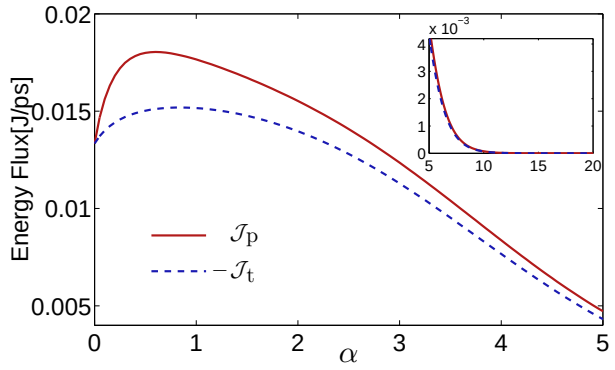

Figure 4: (color online) The steady state pumping (red solid line) and trapping (blue dashed line) energy fluxes versus α. The minus sign in front of the trapping flux suggests the energy flows into the trapping bath. Both fluxes show a maximal value in the weak coupling case and then quickly decreases to zero when α increases. The inset shows the strong coupling case. We use the same parameters of the two level-system as in Fig.3, and the other parameters are chosen as: $\beta_p J = 0.02$, $\beta_t J = 1$, and $\gamma_p/J = \gamma_t/J = 0.01$.

optimal values in the intermediate coupling region and decrease to zero when the coupling strength is strong.

In the context of heat engine, the trapping energy flux $\mathcal{J}_t$ in our model corresponds to the output power and $\mathcal{J}_p$ corresponds to the input power. Usually, the power of a heat engine is small when the efficiency is high. Particularly, at the maximal efficiency, all the processes are required to be quasi-static and take infinite time, and thus the power will be zero. To balance the conflict between the efficiency and power, much work has been done to study the efficiency at maximum power [27–29]. In the following, we will calculate the energy transfer efficiency of our system and show its competitive relation with the trapping flux, in analogy to the efficiency and power in the heat engine.

B. Steady state efficiency

Before presenting the result of efficiency defined in Eq.(6), we begin with the analysis of the limiting cases. The first term on the right side of Eqs.(35)(36) depends only on the populations of the three-level system, and the second term represents the contribution of the off-diagonal terms (coherence in the local basis). As we have showed in Sec III, the steady state coherence in the local bases ρ_{12} vanishes in the strong coupling limit, then the efficiency is completely determined by the populations. According to the steady state solution of the second equation in Eq.(34), we obtain the relation

$$\gamma_p[n_p\rho_{00} - (n_p+1)\rho_{11}] = \gamma_t[(n_t+1)\rho_{22} - n_t\rho_{00}]. \quad (37)$$

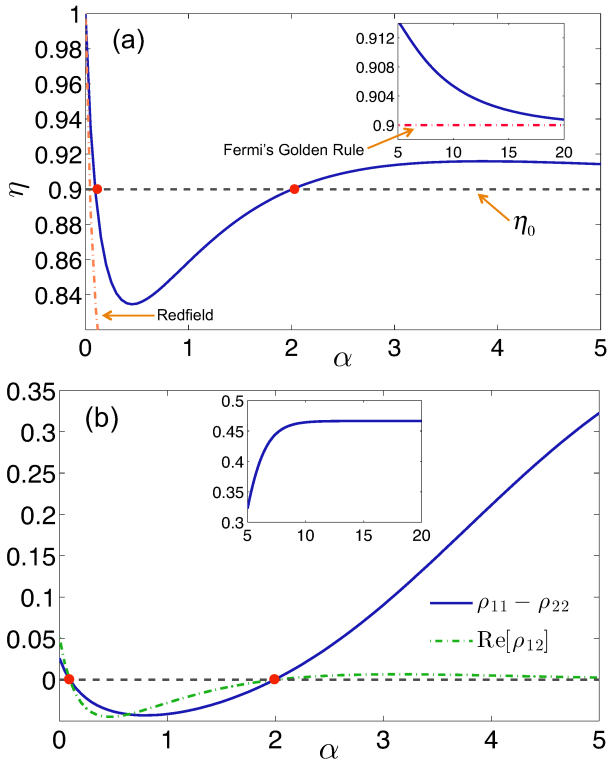

Figure 5: (color online) (a) The steady states efficiency η, (b) the excited states population $\rho_{11} - \rho_{22}$ and coherence $\Re[\rho_{12}]$ versus the system-phonon bath coupling strength characterized by dimensionless parameter α. The dashed line indicates the strong coupling limit η_0 in (a). When the populations are inverted, η is less then η_0, the red dots indicate the corresponding range of α. The results given by the Redfield equation and the Fermi's golden rule are shown with the dashed-dot lines. The strong coupling regions are plotted in the insets. All the parameters are chosen as the same as in Fig.4.

With this relation, the efficiency in the strong coupling limit reads

$$\eta \approx -\frac{\epsilon_2\gamma_t[(n_t+1)\rho_{22} - n_t\rho_{00}]}{\epsilon_1\gamma_p[(n_p+1)\rho_{11} - n_p\rho_{00}]} = \frac{\epsilon_2}{\epsilon_1}. \quad (38)$$

This result indicates that when the coherence is negligible due to the strong system-phonon coupling, the energy transfer efficiency η approaches η_0, which is consistent with the key result of Refs.[12]. We notice that Eq.(37) shows that the net rate of pumping one excitation to $|1\rangle$ equals to the net rate of trapping one excitation from $|2\rangle$ to $|0\rangle$. In general, the efficiency is closely related to the phonon bath induced coherence [30] of the excited states. If we require the system outputs positive energy, i.e., $\gamma_t(n_t+1)\rho_{22} > \gamma_t n_t\rho_{00}$, then according to Eqs.(35)(36)(37), $\Re[\rho_{12}] > 0$ leads to $\eta > \eta_0$ and vise versa.

According to our discussion of the flux in the last subsection, when the coupling strength $\alpha = 0$, the energy transfer efficiency $\eta = 1$ because there is no loss of energy

flux. When the coupling strength gradually increases, the efficiency decreases. However, after reaching its minimum value, the efficiency starts to rise with α, which is shown in Fig.5(a). The increase of efficiency assisted by noise was studied extensively in the context of energy transfer in light-harvesting systems [31–33]. As we further increase α, the efficiency grows beyond the strong coupling limit η_0 and then gradually approaches this limit from above. The strong coupling region is plotted in the inset of Fig.5(a).

Interestingly, we find population inversion of the two excited states in the regimes of $\eta > \eta_0$. We plot the population difference between states $|1\rangle$ and $|2\rangle$ in Fig.5(b). In the intermediate coupling region indicated between the two red dots, the steady state population satisfies $\rho_{11} < \rho_{22}$ (the effective temperature associates with these two states is positive), the corresponding efficiency η is less then η_0 as shown in Fig.5(a). On the contrary, outside this intermediate region, i.e., when the coupling is either very weak or very strong, the populations are inverted $\rho_{11} > \rho_{22}$ (the effective temperature is negative); meanwhile η increase beyond η_0. In the local basis, the population and coherence are coupled with each other due to the polaron effects: The population inversion happens when $\Re[\rho_{12}] < 0$ [Fig.5(b)]. The fact that the population and coherence in the local basis have similar behaviour can be explained from Eq.(31) and Eq.(32). Here, the coherence $\langle \tau_x(t) \rangle_e$ in the polaron basis is negligibly small (see the inset of Fig.3) to have significant effects, then the terms $\langle \sigma_z \rangle = \rho_{11} - \rho_{22}$ and $\langle \sigma_x \rangle = 2\Re[\rho_{12}]$ are both determined by $\langle \tau_z \rangle_e$.

In Fig.5(a), we also compare the efficiency η calculated by the PTRE method with those predicted by the Redfield equation and the Fermi's golden rule approaches. As we mentioned before, in the weak and strong coupling limits, the PTRE method agrees with the Redfield equation and the Fermi's golden rule, respectively, and it connects these two limits with a non-trivial minimum which is related to the coherence in the local basis.

C. Further discussions

1. *kinetic models*

In the strong coupling regime, we can map this energy transfer process into a simple excitation kinetic model as shown in Fig.6(a). Each step of energy transfer is described by an effective flux ($\mathcal{J}_{\rm p}^{\rm eff}$, $\mathcal{J}_{\rm v}^{\rm eff}$ and $\mathcal{J}_{\rm t}^{\rm eff}$). The effective transfer flux $\mathcal{J}_{\rm v}^{\rm eff}$ between the two excited states is approximately proportional to γ_z [Fig.6(b)], which characterizes the relaxation rate of the two excited states. When $\mathcal{J}_{\rm v}^{\rm eff}$ (or γ_z) is smaller than the trapping flux $\mathcal{J}_{\rm t}^{\rm eff}$ (or $\gamma_{\rm t}$), the excitation in excited states will be quickly captured by the trapping field without enough time to first get equilibrated with the phonon bath. Consequently, the populations of the two excited states are inverted and the real part of the coherence becomes negative. This phenomenological mechanism explains why the efficiency η is higher than η_0 in the strong coupling limit.

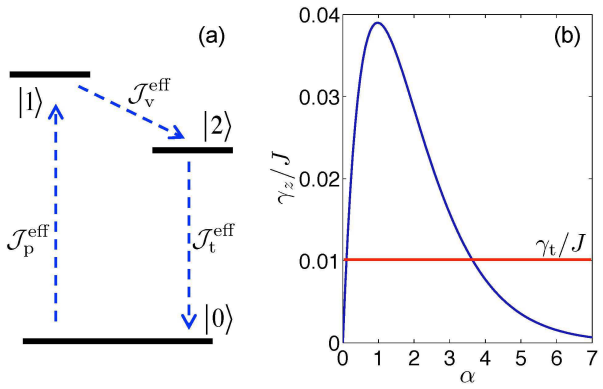

Figure 6: (color online) (a) The kinetic model of a single excitation transfer cycle. In the strong coupling regime, the energy transfer processes between different local states can be described by the effective fluxes. (b) The transfer rate γ_z versus system-bath coupling strength α. The red line indicates the trapping rate $\gamma_{\rm t}$. The parameters here are the same with Fig.4.

When the system-bath coupling strength becomes weaker, the local basis frame is no longer a good option for the kinetic picture. The two excited states couple with each other and can be together considered as an excited state manifold, as shown in Fig.7(a). The single excitation carrying certain amount of energy passes through the excited states $|1\rangle$ and $|2\rangle$, and its average residence time $\langle t \rangle$ in the excited states is negatively correlated with the transfer efficiency (in analogy to the light-harvesting efficiency in Ref.[33, 34]): i.e., the longer the excitation stays in the excited states, the more energy will be lost to the phonon bath, and the lower energy transfer efficiency will be. During a cycle that the single excitation starts from $|0\rangle$ and finally returns to $|0\rangle$, the average residence time $\langle t \rangle$ is proportional to the excited states population $\rho_{11} + \rho_{22}$ at the steady states, as shown in Fig.7(b). Though not quantitively exact, this kinetic model qualitatively explains the local minimal of the efficiency η via the average residence time $\langle t \rangle \sim \rho_{11} + \rho_{22}$.

2. *temperature dependence*

Besides the system-phonon bath coupling strength, the temperature of the phonon bath also affects the energy transfer process, as shown in the two-dimensional contours of energy transfer efficiency [Fig.8(a)] and trapping energy flux [Fig.8(b)]. The efficiency behaves the same at the high phonon bath temperature as in the strong coupling. In the high temperature limit, even when the coupling strength is weak, the efficiency is still close to η_0. As seen from Eq.(12), in either limit $\alpha \to \infty$ or $\beta_{\rm v} \to 0$, the renormalization factor $\kappa \to 0$; therefore, ex-

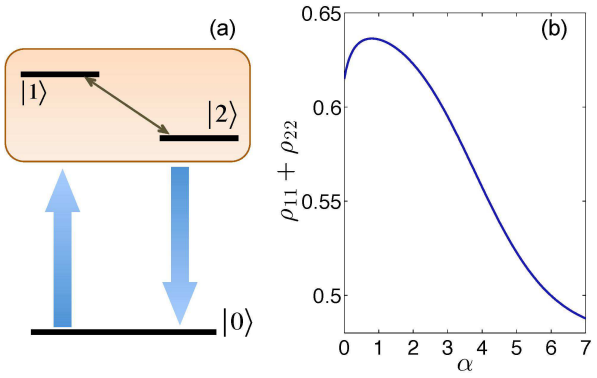

Figure 7: (a) The two excited states form a black box for the input and output excitation due to the internal coupling. (b) The average residence time $\langle t\rangle$ is proportional to the total population of the excited states. The parameters here are also the same as those in Fig.4.

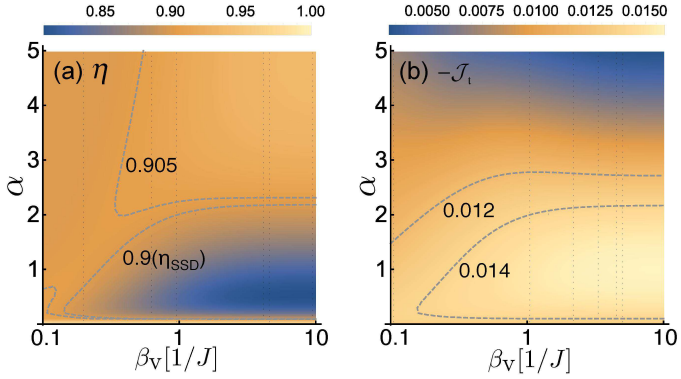

Figure 8: (color online) The dependence of (a) the energy transfer efficiency and (b) the trapping energy flux on the coupling strength and temperature of the phonon bath. The temperatures and dissipation coefficients of the pumping and trapping bath are the same as in the Fig.5.

cept for the weak coupling and low temperature case, the efficiency η does not change obviously.

The trapping energy flux has a different temperature dependences for weak and strong system-bath couplings. The flux $-\mathcal{J}_t$ grows (goes down) with descending β_v when α is small (large). Moreover, $-\mathcal{J}_t$ does not sensitively depend on β_v with small α in contrast with the efficiency. When the coupling α is around 1, the flux $-\mathcal{J}_t$ changes no more than 20% in amplitude comparing with its maximum. The optimization of the efficiency and the trapping flux can be achieved in two different regimes: 1) The coupling strength is weak and the temperature of the phonon bath is high. 2) The coupling strength is medium ($\alpha \sim 2.5$) and the bath temperature is low (β_v>1). The first regime corresponds to the high temperature classical limit, and the second regime corresponds to low-temperature quantum regime, where bath-induced coherence enhances the energy transfer process.

V. CONCLUSION

In this paper we use the polaron transformed Redfield equation (PTRE) to analyze the effects of the phonon bath on the energy transfer process in a generic three-level model. As a quantitative method, the PTRE can reliably describe the dependence of the steady state coherence on the system-bath coupling strength ranging from the weak to strong coupling regime. Our analysis shows that the steady state coherence between the two excited states is crucial to the energy transfer efficiency. When the effective temperature of the excited states is negative (populations are inverted), the coherence carries a positive real part and enhances the efficiency beyond the strong coupling limit η_0. On the contrary, if the effective temperature is positive (populations are not inverted), the coherence carries a negative real part and is detrimental to the efficiency. The energy flux and efficiency compete with each other and cannot reach maximum simultaneously; however, the study of their behaviours with respect to the coupling strength and temperature provides the key information about how to make an optimal compromise between the two quantities. We will consider how to use quantum control to optimize the energy transfer process in the future study.

Acknowledgments

DX and YZ were supported by the National Research Foundation, Republic of Singapore, through the Competitive Research Program (CRP) under Project No. NRF-CRP5-2009-04. JC acknowledges the National Science Foundation (NSF) of the US (grant no. CHE-1112825). CW has been supported by the Singapore-MIT Alliance for Research and Technology (SMART).

Appendix A M and $\vec{C}$ in Eq.(23) and Eq.(24)

The quantities defined in Eq.(23) and Eq.(24) are determined by the superposition of the correlation functions Eq.(19) following Eqs.(13)(22). The straightforwardly calculation gives:

$$\begin{aligned}
\gamma_z &= \frac{1}{2}\kappa^2 J^2 \int_0^\infty dt \cos(\Delta t)\left[f(t)\cos^2\theta + g(t)\right], \\
\gamma_x &= \frac{1}{2}\kappa^2 J^2 \int_0^\infty dt \left[f(t)\sin^2\theta + \cos(\Delta t)\, g(t)\right], \\
\gamma_y &= \frac{1}{2}\kappa^2 J^2 \int_0^\infty dt f(t)\left[\cos^2\theta\cos(\Delta t) + \sin^2\theta\right], \\
\gamma_{zx} &= \frac{1}{4}\kappa^2 J^2 \sin 2\theta \int_0^\infty dt f(t), \\
\gamma_{xz} &= \frac{1}{4}\kappa^2 J^2 \sin 2\theta \int_0^\infty dt f(t)\cos(\Delta t),
\end{aligned}$$

$$
\begin{aligned}
\gamma_{xy} &= \frac{1}{2}\kappa^2 J^2 \int_0^\infty dt g(t)\sin(\Delta t),\\
\gamma_{yx} &= -\frac{1}{2}\kappa^2 J^2 \cos^2\theta \int_0^\infty dt f(t)\sin(\Delta t),\\
\gamma_{yz} &= \frac{1}{4}\kappa^2 J^2 \sin 2\theta \int_0^\infty dt f(t)\sin(\Delta t),\\
C_z &= -\frac{i}{2}\kappa^2 J^2 \int_{-\infty}^\infty dt \sin(\Delta t)\\
&\quad \times \left[\cos^2\theta\cosh[Q(t)] + \sinh[Q(t)]\right],\\
C_x &= -\frac{i}{4}\kappa^2 J^2 \sin 2\theta \int_{-\infty}^\infty dt \sin(\Delta t)\cosh[Q(t)],\\
C_y &= -\frac{i}{4}\kappa^2 J^2 \sin 2\theta \int_0^\infty dt [1-\cos(\Delta t)]\\
&\quad \times [\cosh[Q(t)] - \cosh[Q(-t)]],
\end{aligned}
$$

where

$$
\begin{aligned}
f(t) &= \cosh[Q(t)] + \cosh[Q(-t)] - 2,\\
g(t) &= \sinh[Q(t)] + \sinh[Q(-t)].
\end{aligned}
$$

Using the super-Ohmic spectrum $J(\omega) = \alpha\pi\omega^3\omega_c^{-2}e^{-\omega/\omega_c}$, the function $Q(t)$ reads

$$
\begin{aligned}
Q(t) &= \int_0^\infty d\omega \frac{J(\omega)}{\pi\omega^2}\left[(2n_{\rm v}(\omega)+1)\cos(\omega t) - i\sin\omega t\right]\\
&= \alpha\left\{\frac{-1+\omega_c^2 t^2 - i2\omega_c t}{(1+\omega_c^2 t^2)^2} + \frac{2\Re\left[\psi_1\left(\frac{1}{\beta_{\rm v}\omega_c}+\frac{it}{\beta_{\rm v}}\right)\right]}{(\beta_{\rm v}\omega_c)^2}\right\}.
\end{aligned}
$$

Appendix B $\bar{M}$ in Eq.(34)

The Liouville operator $\mathcal{L}_{\rm v}$ for the three-level system is obtained from Eq.(22) for the TLS with the expressions in Appendix A. Here the relation $\rho_{00}+\rho_{11}+\rho_{22}=1$ should be used to substitute $[\rho_e]_{11}+[\rho_e]_{22}=1$ for the TLS. Taking the contributions of the Lindblad terms $\mathcal{L}_{\rm p}$ and $\mathcal{L}_{\rm t}$ defined in Eq.(7) into consideration, the elements of the matrix $\bar{M}$ in Eq.(34) are

$$
\begin{aligned}
\bar{M}_{11} &= \gamma_z\cos^2\theta + \gamma_x\sin^2\theta + \frac{1}{2}(\gamma_{xz}+\gamma_{zx})\sin 2\theta\\
&\quad + \frac{1}{2}[\gamma_{\rm p}(n_{\rm p}+1) + \gamma_{\rm t}(n_{\rm t}+1)],\\
\bar{M}_{12} &= -C_z\cos\theta - C_x\sin\theta + \frac{1}{2}[\gamma_{\rm p}(3n_{\rm p}+1) - \gamma_{\rm t}(3n_{\rm t}+1)],\\
\bar{M}_{13} &= \kappa^{-1}[\gamma_{xz}\sin^2\theta - \gamma_{zx}\cos^2\theta + \frac{1}{2}(\gamma_z-\gamma_x)\sin 2\theta],\\
\bar{M}_{14} &= -\kappa^{-1}(\Delta+\gamma_{xy})\sin\theta,\\
\bar{M}_{21} &= \frac{1}{2}[\gamma_{\rm p}(n_{\rm p}+1) - \gamma_{\rm t}(n_{\rm t}+1)],\\
\bar{M}_{22} &= \frac{1}{2}[\gamma_{\rm p}(3n_{\rm p}+1) + \gamma_{\rm t}(3n_{\rm t}+1)],\\
\bar{M}_{23} &= \bar{M}_{24} = 0,\\
\bar{M}_{31} &= \kappa[\gamma_{zx}\sin^2\theta - \gamma_{xz}\cos^2\theta + \frac{1}{2}(\gamma_z-\gamma_x)\sin 2\theta],\\
\bar{M}_{32} &= \kappa(C_x\cos\theta - C_z\sin\theta),\\
\bar{M}_{33} &= \gamma_x\cos^2\theta + \gamma_z\sin^2\theta - \frac{1}{2}(\gamma_{xz}+\gamma_{zx})\sin 2\theta\\
&\quad + \frac{1}{2}[\gamma_{\rm p}(n_{\rm p}+1) + \gamma_{\rm t}(n_{\rm t}+1)],\\
\bar{M}_{34} &= (\Delta+\gamma_{xy})\cos\theta,\\
\bar{M}_{41} &= \kappa[(\Delta-\gamma_{yx})\sin\theta - \gamma_{yz}\cos\theta],\\
\bar{M}_{42} &= \kappa C_y,\\
\bar{M}_{43} &= -(\Delta-\gamma_{yx})\cos\theta - \gamma_{yz}\sin\theta,\\
\bar{M}_{44} &= \gamma_y + \frac{1}{2}[\gamma_{\rm p}(n_{\rm p}+1) + \gamma_{\rm t}(n_{\rm t}+1)].
\end{aligned}
$$

[1] G. S. Engel, T. R. Calhoun, E. L. Read, T.-K. Ahn, T. Mancal, Y.-C. Cheng, R. E. Blankenship, and G. R. Fleming, Nature **446**, 782 (2007).
[2] A. Ishizaki and G. R. Fleming, Proc. Natl. Acad. Sci. **106**, 7255 (2009).
[3] J. L. Wu , F. Liu, Y. Shen, J. Cao, and R. J. Silbey, New J. Phys. **12** 105012 (2010).
[4] T. V. Tscherbul and P. Brumer, Phys. Rev. Lett. **113**, 113601 (2014).
[5] J. Olšina, A. G. Dijkstra, C. Wang and J. Cao, arXiv:1408.5385 (2014).
[6] H. T. Quan, Y. X. Liu, C. P. Sun, and F. Nori, Phys. Rev. E **76**, 031105 (2007).
[7] M. O. Scully, K. R. Chapin, K. E. Dorfman, M. B. Kim, and A. Svidzinsky, Proc. Natl. Acad. Sci. **108** (37), 15097 (2011).
[8] K. E. Dorfman, D. V. Voronine, S. Mukamel, and M. O. Scully, Proc. Natl. Acad. Sci. **110** (8), 2746 (2011).
[9] H. E. D. Scovil and E. O. Schulz-DuBois, Phys. Rev. Lett. **2**, 262 (1959).
[10] J. E. Geusic, E. O. Schulz-DuBois and H. E. Scovil, Phys. Rev. **156**, 343 (1967).
[11] E. Geva and R. Kosloff, J. Chem. Phys. **104**, 7681 (1996).
[12] E. Boukobza, and D. J. Tannor, Phys. Rev. A **74**, 063823 (2006).
[13] E. Boukobza, and D. J. Tannor, Phys. Rev. Lett. **98**, 240601 (2007).
[14] N. Linden, S. Popescu, and P. Skrzypczyk, Phys. Rev. Lett. **105**, 130401 (2010).
[15] A. Levy and R. Kosloff, Phys. Rev. Lett. **108**, 070604 (2012).
[16] S. Rahav, U. Harbola, and S. Mukamel, Phys. Rev. A **86**, 043843 (2012).
[17] L. A. Correa, J. P. Palao, D. Alonso, G. Adesso, Sci. Rep. **4**, 3949 (2014).
[18] H. Dong, S. Yang, X. F. Liu, and C. P. Sun, Phys. Rev. A **76**, 044104 (2007).
[19] H. Dong, X. F. Liu, and C. P. Sun, Chin. Sci. Bull. **55**,

3256 (2010).
[20] C. K. Lee, J. Cao, and J. B. Gong, Phys. Rev. E **86**, 021109 (2012).
[21] C. K. Lee, J. Moix, and J. Cao, J. Chem. Phys. **136**, 204120 (2012).
[22] D. Z. Xu, S. W. Li, X. F. Liu, and C. P. Sun, Phys. Rev. E **90**, 062125 (2014).
[23] M. Grover and R. J. Silbey, J. Chem. Phys. **54**, 4843 (1971).
[24] R. J. Silbey and T. Harris, J. Chem. Phys. **80**, 2615 (1984).
[25] C. Wang, J. Ren and J. Cao, Scientific Reports, **5**, 11787 (2015).
[26] C. Wang, J. Ren, and J. Cao, New J. Phys. **16**, 045019 (2014).
[27] F. Curzon and B. Ahlborn, Am. J. Phys. **43**, 22 (1975).
[28] C. Van den Broeck, Phys. Rev. Lett. **95**, 190602 (2005).
[29] M. Esposito, K. Lindenberg and C. Van den Broeck, Phys. Rev. Lett. **102**, 130602 (2009).
[30] A. G. Dijkstra, C. Wang, J. Cao, and G. R. Fleming, J. Phys. Chem. Lett. **6**, 627 (2015).
[31] F. Caruso, A. W. Chin, A. Datta, S. F. Huelga and M. B. Plenio, J. Chem. Phys. **131**, 105106 (2009).
[32] P. Rebentrost, M. Mohseni, I. Kassal, S. Lloyd and A. Aspuru-Guzik, New J. Phys. **11**, 033003 (2009).
[33] J. Cao and R. J. Silbey, J. Phys. Chem. A **113**, 13826 (2009).
[34] J. Wu, R. J. Silbey, and J. Cao, Phys. Rev. Lett. **110**, 200402 (2013).